UC Berkeley
UC Berkeley Previously Published Works

Title
On the design of random metasurface based devices.

Permalink
https://escholarship.org/uc/item/3sp69804

Journal
Scientific reports, 8(1)

ISSN
2045-2322

Authors
Dupré, Matthieu
Hsu, Liyi
Kanté, Boubacar

Publication Date
2018-05-01

DOI
10.1038/s41598-018-25488-4

Peer reviewed

SCIENTIFIC REPORTS

On the design of random metasurface based devices

Matthieu Dupré, Liyi Hsu & Boubacar Kanté

Metasurfaces are generally designed by placing scatterers in periodic or pseudo-periodic grids. We propose and discuss design rules for functional metasurfaces with randomly placed anisotropic elements that randomly sample a well-defined phase function. By analyzing the focusing performance of random metasurface lenses as a function of their density and the density of the phase-maps used to design them, we find that the performance of 1D metasurfaces is mostly governed by their density while 2D metasurfaces strongly depend on both the density and the near-field coupling configuration of the surface. The proposed approach is used to design all-polarization random metalenses at near infrared frequencies. Challenges, as well as opportunities of random metasurfaces compared to periodic ones are discussed. Our results pave the way to new approaches in the design of nanophotonic structures and devices from lenses to solar energy concentrators.

Originally designed at radio wave frequencies for radar and space communications[1–5], metasurfaces have been implemented to design devices at visible and infrared wavelengths such as carpet cloaks[6–9], holograms[10–17], optical flat lenses[18–21] and solar concentrators[22,23] to name a few. Metasurfaces control the reflection and refraction of waves at interfaces using phase-shifting elements[24]. In optics, whether they are designed from metallic materials using plasmonic phenomena[7,18,24–29] or dielectrics to obtain higher efficiencies at the cost of larger elements[20,22,30,31], whether they are relying on subwavelength gratings[32,33], resonators[7,22,24,27,28], waveguides[19,26,31] and, or, geometric phase[18,20,26,32,34,35] to tune the phase of the wave, metasurfaces are generally designed in a periodic framework where their constituting elements are placed in a periodic grid[30].

Recent advances on the control of light in complex media[36] have motivated the study of random or disordered metasurfaces for specific applications such as decreasing the radar cross-section[37–40], improving SERS enhancement[41], reducing laser coherence[42], designing wide band-gaps[43], or increasing light-matter interaction and the absorption of solar cells[44,45]. One of the advantages of random media is the very high number of degrees of freedom that they support and which can be harnessed to control waves on scales smaller than the wavelength, or to multiplex more information for communication[36,46]. This has recently led to the design of random metasurfaces for wave front shaping[47–49]. However, the design of such devices still remains elusive due to the disordered distances between neighboring elements, the near-field coupling, and variations of the local density of elements. Some theoretical approaches can address the homogenization problem of homogeneous random polarizability materials in periodic arrays of resonators[50], or for identical polarizabilities in disordered arrays of scatterers[51,52].

The relation providing the phase-shift of the elements constituting a metasurface as a function of their dimensions is determined either analytically, when possible, or with numerical simulations for a single element or for periodic arrays of identical elements. However, metasurfaces are generally made of elements of different sizes to provide a phase-shift that varies spatially. Hence, the previous approaches may fail[53] as near-field coupling introduces errors in the phase-shifts provided by the elements. Important questions are thus whether this periodic arrangement is always the best solution and whether it is possible to design functional metasurfaces within a random framework with general guidelines.

While random and disordered metasurfaces can be complex to design, they also have potential advantages. For instance, the random design process optimizes the area of the metasurface. In a periodic metasurface, small and large elements have the same footprint. On the contrary, in a random metasurface, the random design or the pseudo random algorithm finds more easily a spot for a small element than for a larger one. This optimizes the local density and the footprint of the elements. Furthermore, the absence of periodicity eliminates any spurious diffraction orders that arise from large periods[54], due for example to large resonators made of low index materials. The circular symmetry of the elements is also statistically restored by the randomness[55], which enables the design of polarization independent metalenses with anisotropic elements. This contrasts with the

UC San Diego, Department of Electrical and Computer Engineering, 9500 Gilman Drive, La Jolla, CA, 92093, USA. Correspondence and requests for materials should be addressed to B.K. (email: bkante@ucsd.edu)
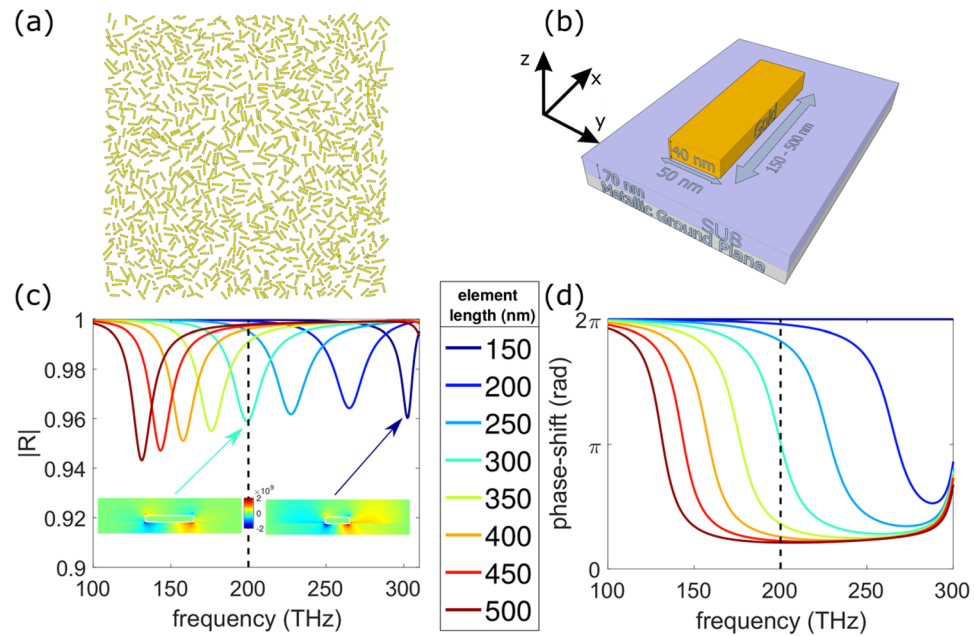
Figure 1. (**a**) Random metalens made of gold anisotropic scatterers. (**b**) Phase-shifting element (nano-resonator) of the metasurface. The element dimensions are 50 nm width, 40 nm height, with a length varying from 150 nm to 500 nm. The dielectric spacer, SU8, has a thickness of 70 nm and is on a metallic ground plane. (**c**) Amplitude of the reflection coefficient as a function of the frequency around 200 THz and for elements length from 150 nm to 500 nm. Vertical dashes mark the 200 THz frequency. $p_x = 900$ nm and $p_y = 100$ nm. Insert: Electric field (z component) in the plane ($y = 0$ nm) of the 150 nm at 300 THz and the 300 nm element at 200 THz. (**d**) Same as (**c**) for the phase-shift of the reflection coefficient.

current works implementing polarization independent lenses using circular or fourfold symmetric cross-section elements[19,31,56–58].

Here, using anisotropic gold nano-elements as resonators, we design random metasurface lenses at the wavelength of $\lambda_0 = 1.5$ μm. Such metasurfaces are designed using randomly sampled elements, which lengths are computed in order to provide the required phase law at each of the sampled position. To establish general rules and guidelines for such designs, the resonators are first considered in a periodic framework to numerically obtain their phase maps $\phi(l)$, i.e. the phase-shift provided by the element as a function of a geometrical parameter—the length in our case—for different periods of the array. These periods, corresponding to a density of the phase-map, are then used as references from which a resonator can be chosen. Then, using different phase-maps, one-and two dimensional metasurfaces of periodic or random elements of various densities can be constructed. The performances of the designs are then discussed.

Results

Phase-maps and unit cell simulations. To design random metalenses such as the one represented in Fig. 1(a), phase-shifting elements need to be used. Figure 1(b) presents a possible implementation using anisotropic gold nano-resonators. The elements has a width of 50 nm, a height of 40 nm, and the length is tuned between 150 nm and 500 nm. Gold is modeled using a Drude model with a plasma frequency $\omega_p = 1.367 \times 10^{16}$ rad/s and a collision frequency $\omega_c = 6.478 \times 10^{13}$ rad/s[59]. This plasmonic particle is supported by a dielectric SU8 spacer with a refractive index $n_{SU8} = 1.59$, optimized to a thickness of 70 nm, on top of a metallic ground plane (more details in supplementary information).

The building block of the metasurfaces is first investigated using in-plane periodic boundary conditions, as shown in Fig. 1(b). The period in the direction of the width of the element (period p_y in the y direction) will be swept but is kept to 100 nm in Fig. 1. The period along the longer dimension of the element (p_x in the x direction) is set to 900 nm and is kept constant all along the paper. Using the frequency domain solver of the commercial software CST, the complex reflection coefficient of our structure is computed. The illuminating plane wave has a frequency varying from 50 THz to 350 THz and is polarized along x (i.e. the long axis of the particle). The particle is transparent to the orthogonal polarization (see supplementary information). Varying the length of the particle from 150 nm to 500 nm shifts its fundamental resonance frequency as shown in Fig. 1(c). The phase of the wave reflected by the particle and the metallic plane can thus be controlled. It is worth noting that there is no transmission because of the metallic ground plane and the absorption is 1-R. Figure 1(d) shows the phase shift of an element around 200 THz ($\lambda_0 = 1500$ nm) for different particle lengths. The shortest element is taken as phase reference. Figure 2(a) shows the phase shift as a function of the length of the elements for different periods p_y at 200 THz. For a single resonance, the complete 2π phase shift is only obtainable asymptotically far away from the resonance. The SU8 spacer thickness sets the quality factor Q of the resonances which in turn, controls the
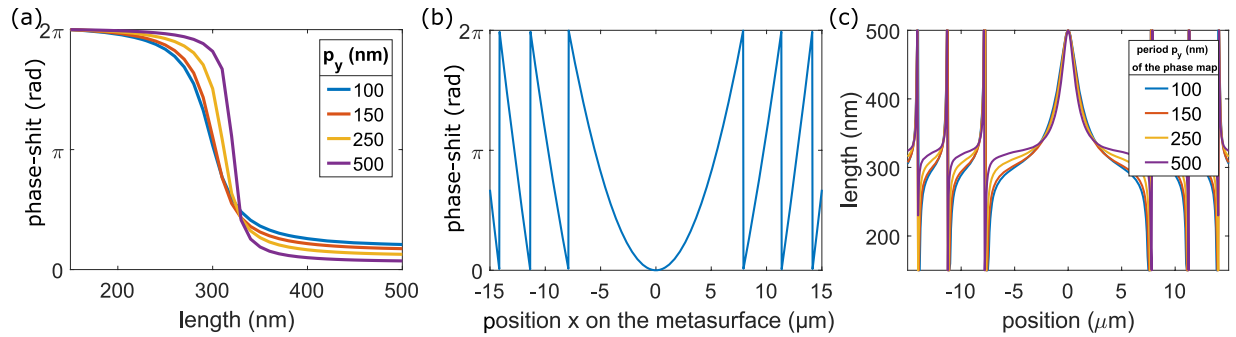
Figure 2. (**a**) Phase-maps for different periods p_y (100, 150, 200, 500 nm): Phase shift provided by an element at 200 THz as a function of the length of the element. (**b**) Phase shift required as a function of the position, to design a lens of 30 μm width with a focal length of 20 μm at 200 THz. (**c**) Length of the elements as a function of the position to design the lens. Curves are obtained from (**a**) and (**b**) for different periods p_y (along the short dimension of the elements).

maximum value of the phase-shift—the thicker the SU8 layer, the lower the Q factor and the smaller the maximum phase-shift. However, the higher the Q factor, the sharper the slope of the reflected phase. Hence, a compromise has to be made between the maximum value of the phase shift and the slope of the reflected phase around 200 THz (Fig. 1(d)). A very steep change of phase introduces phase errors[22,53]. A thickness of 70 nm (the red curve on Fig. 2(a)) appears to be a good compromise as the difference between 2π and the maximum phase-shift is smaller than 37°.

The phase-shift required to design a parabolic lens in reflection or concentrator with a focal length f is given by the parabolic law[22,27]:

$$\varphi(x) = k_0 \left(\sqrt{x^2 + f^2} - f \right) \tag{1}$$

The phase-shift required to design a metalens of 30 μm width with a focal spot of 20 μm is shown in Fig. 2(b). Knowing the phase-shift required at any position of the metasurface (Fig. 2(b)) and the phase shift induced at reflection on a periodic array as a function of the element length (Fig. 2(a)) (reference phase-map), leads to choose the length of the elements as a function of their position on the metasurface. Figure 2(c) presents the length required at a given position to realize the phase shift plotted in Fig. 2(b), for different phase-maps represented by different periods p_y (from 150 nm to 500 nm) in the periodic array. Changing the period shifts the phase of the field reflected by an array of identical elements. This originates from two reasons: the near-field coupling that becomes stronger as the distance between the elements is decreased, and the density of elements itself in the limit of negligible near-field coupling. Indeed, the denser the array, the more field will be phase-shifted by the elements compared to the field which is only reflected by the ground plane. The total reflected field which is the sum of the field reflected by the mirror and the field scattered by the elements has therefore different phases for different densities. The two insets of Fig. 2(c) show the "z" component of the electric field in the near field of the elements of 300 nm length and 150 nm at their resonant frequency (respectively 200 and 300 THz).

One-dimensional random metalenses. For a periodic metasurface, on one hand, choosing a period p_y of a phase-map sets the density of elements per unit area of the periodic array: the relation between the period and the density is: $\rho = 1/p_x p_y$. On the other hand, the main questions that arise are which density optimizes the focusing of a random metalens, and which phase-map should be chosen to design a metasurface at this density. A naïve response would be to select the phase-map with the same density as the random metasurface to be designed, but, as will be seen later, the response is not straightforward. These questions are all the more important that random metasurfaces have fluctuations of the near-field coupling that may affect the efficiency if the density becomes too high.

We simulated 16 different random metasurfaces corresponding to four densities of phase-maps (four periods in the y direction (p_y) of 100 nm, 150 nm, 250 nm and 500 nm) and four equivalent densities in the random metasurface of 25, 17, 10 and 5 elements per squared wavelength. On a matrix with the rows representing the density of the phase-maps and the columns representing the density of the random metasurface, elements on the diagonal are thus those for which the two densities are equal. Figure 3 represents 16 one-dimensional metasurfaces with a width (along "y") of 30 μm and a focal length (along "z") of 20 μm. Elements are set along "x" perpendicularly to the 1D metasurface (Fig. 3(a), out of plane of the Fig. 3(b)). Periodic boundary conditions define the out of plane direction, with a period of 900 nm.

Our algorithm to design a random metasurface corresponds to random loose packing[60] and consists in the following steps. First, we randomly select a position (for 2D metasurfaces, we also choose a random orientation for the element). For 1D metasurfaces, all elements are parallel to their longest length. We compute, using the phase maps of Fig. 2(a–c) the length that a particle at this position should have. We then check if it is overlapping or is too close to previously placed elements. A minimum distance between the surfaces of the elements of 10 nm is set in order to put the elements as close as possible to get the maximum density but this value can be varied. If the minimum distance between elements is too small or if they overlap, we remove it and select another random
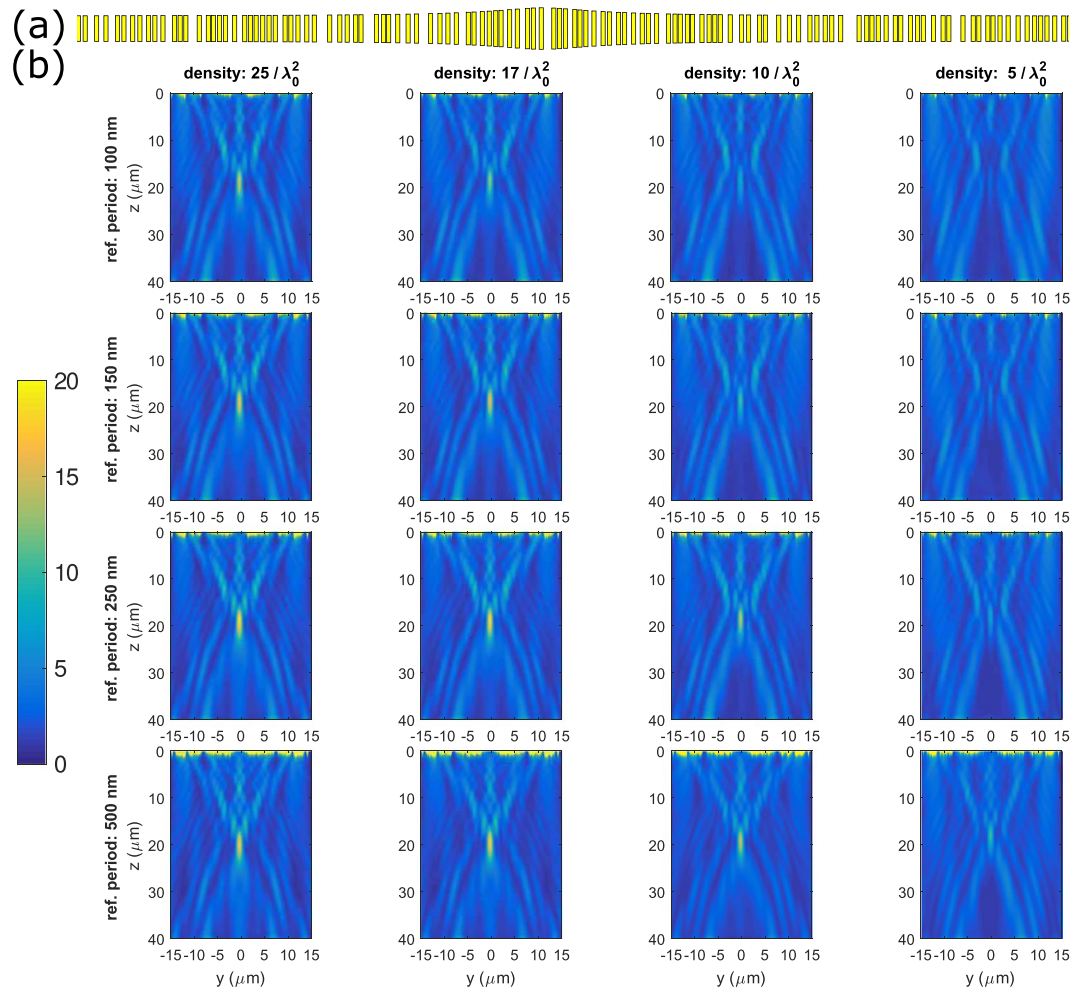
Figure 3. (**a**) Example of 1D random metasurface realization for the highest density in the plane z = 0. (**b**) Average of the density of energy over 10 samples of 1D random metasurfaces. Density of energy of the reflected field normalized by the density of energy of the incident field plotted in the *yz* plane for 16 one-dimensional random metalenses at 200 THz (λ = 1.5 μm) corresponding to four different periods of the reference times four different but equivalent densities of the random metasurface. The considered densities are 25, 17, 10, 5 λ_0^{-2}, and they correspond to periods p_y in the periodic system of 100 nm, 150 nm, 250 nm, and 500 nm.

position. If they do not overlap, we approve the change and move to the next particle. The process is repeated until we manage to place a defined number of elements (from 300 for a density of 25 λ_0^{-2} to 60 for a density of $5\lambda_0^{-2}$) or until we have failed to place a given element. This would mean that the maximal density of the random metasurface has been reached. Using CST simulations in time domain for better computational efficiency, we computed the density of energy of the reflected field normalized by the density of energy of the incident plane wave for the sixteen 1D random metasurfaces. Each design is randomly repeated, simulated ten times, and averaged to ensure that the results are statistically meaningful. The average results for the 16 (4 by 4) metasurfaces are displayed on Fig. 3. Unaveraged results are very similar as the maximum value of the standard deviation is found to be about 10% of the average value (see supplementary information).

Figure 3 presents the density of reflected energy normalized to the density of incident energy for the 16 metasurfaces. Metasurfaces on the diagonal of the figure and below the diagonal have better focusing performance, i.e. higher energy at the focal spot, than those above the diagonal. This impression is confirmed by the measured values in Table 1. This figure and its table show that for the designed 1D random metasurfaces, the density of elements in the metasurface plays a more important role than the density of the particular phase-map chosen to design the metasurface. This is an interesting conclusion as near-field coupling fluctuation in the random system, when the phase-map is no longer representative of the metasurface, does not seem to alter the focusing ability of the metasurface.

Two-dimensional random metalenses. We now consider 2D metalenses. As in the 1D case, metasurfaces are constructed using the same phase-maps corresponding periods p_y of the reference of 100 nm, 150 nm, 250 and 500 nm. The size of the 2D metasurfaces is chosen to be 10 by 10 μm, with a focal length of 10 μm to limit the computational volume. The phase shift provided by the elements is now a function of *x* and *y*. The nominal frequency is still 200 THz ($\lambda_0 = 1.5$ μm). We again simulate 10 sets of 16 metasurfaces with densities from 25 λ_0^{-2}

	Metric	Dens. $25/\lambda_0^2$	Dens. $16/\lambda_0^2$	Dens. $10/\lambda_0^2$	Dens. $5/\lambda_0^2$
Ref. period: 100 nm	Max(U)	23 ± 1.2	19 ± 2.8	16 ± 1.9	8.9 ± 1.5
	ΔX (μm)	1.37 ± 0.05	1.3 ± 0.1	1.34 ± 0.05	1.4 ± 0.2
	ΔZ (μm)	10 ± 0.15	10 ± 0.3	11 ± 1.3	13 ± 0.9
Ref. period: 150 nm	Max(U)	22 ± 1.5	21 ± 2.2	16 ± 2.2	11 ± 2.3
	ΔX (μm)	1.38 ± 0.06	1.37 ± 0.05	1.4 ± 0.1	1.44 ± 0.15
	ΔZ (μm)	10.1 ± 0.15	10.2 ± 0.2	11 ± 1.6	13 ± 0.7
Ref. period: 250 nm	Max(U)	22 ± 1.8	19 ± 1.9	18 ± 1.4	13 ± 2.9
	ΔX (μm)	1.46 ± 0.07	1.44 ± 0.08	1.40 ± 0.07	1.5 ± 0.09
	ΔZ (μm)	10.2 ± 0.3	10.4 ± 0.2	10.1 ± 0.5	11.7 ± 1.8
Ref. period: 500 nm	Max(U)	11.2	15 ± 1.2	13 ± 2.5	10 ± 2.3
	ΔX (μm)	1.6 ± 0.1	1.6 ± 0.1	1.6 ± 0.2	1.8 ± 0.6
	ΔZ (μm)	11.2 ± 0.3	11.1 ± 0.8	11.3 ± 2	12.4 ± 3

Table 1. Summary of the performances of the 1D random metasurfaces with the mean maximum density of energy, width and length of the focal spots, with their standard deviations.

to $5\,\lambda_0^{-2}$ and present the averaged results. The process to design the random metalenses is the same as for the 1D case, but with randomly placed and oriented elements as shown in Fig. 1(a). A minimum distance between the surfaces of the elements of 10 nm between adjacent elements is enforced and makes the structures realistic to fabricate.

The focusing results, i.e., the reflected density of energy in the plane $y = 0$, which corresponds to a cross section of the central volume, are shown in Fig. 4, while Table 2 displays the main characteristics of the focal spots. Metasurfaces produce well defined focal spots of 1.9 μm by 8 μm, i.e. slightly superior to Abbe's limit $\lambda_0/2NA = 1.6$ μm and $\lambda_0/NA^2 = 6$ μm. Very interestingly, the best results are not achieved anymore for metasurfaces below the diagonal. This contrasts with the 1D case, where metasurfaces of the lower-left part of the figure, i.e. which are designed for equal or higher densities than their corresponding phase-maps, provided good results. Here the three best results are obtained with the densest phase-map with $p_y = 100$ nm. With this phase-map density, even the random metasurface with a density of $5/\lambda_0^2$ leads to a visible focusing spot. The density of the phase-maps thus seems to play a more important role than the density of the random metasurface itself even if the two parameters obviously play a role. The phase shift in denser phase-maps accounts for a more important near-field coupling between elements. Near-field coupling thus seems to play a more important role in the designed 2D random metasurfaces than in the design of 1D metasurfaces. In 2D metasurfaces the elements are randomly oriented whereas they were all aligned in the 1D random metasurfaces. Near-field interactions in 2D metasurfaces are different from what is modeled in the phase-maps and thus raises fundamental questions on the optimal design of random metasurfaces. As noted in a recent paper[53], near-field interactions between adjacent elements in a gradient metasurface do not account for the fact that elements are different, because phase-maps use identical elements. This problem is exacerbated in metasurfaces in which the cross-talk between elements is not negligible. While ideas to address this problem and improve the efficiency were proposed for gradient metasurfaces using periodic grids[53], the question still remains open for random structures that thus operate away from their optimum.

It is worth underlining that near-field coupling is present in both 1D and 2D metasurfaces. However, in 1D metasurfaces, near-field coupling is well accounted for by phase-maps from simulations with periodic and aligned structures. Randomly oriented elements in 2D metasurfaces lead to near-field coupling that deviates more from the phase-maps simulations. Even if 2D near-field coupling is in average weaker than 1D near-field coupling (the coupling being stronger for collinear dipoles), the use of the proposed phase-maps leads to a stronger dependence of the 2D metasurface on the scatterers configuration.

Discussion

In the previous section, we have proposed a strategy to design 2D random metasurface lenses. A 2D random metasurface using anisotropic elements such as rectangle elements are expected to be polarization independent, an important property for many applications. The theoretical focusing power of the 2D random metasurfaces is expected to be half of the focusing power of the corresponding periodic 2D metasurface using the same anisotropic element. However, there is not a one to one map between the periodic and the random structure of the same density as near-field coupling between elements in the two surfaces is different. We present in supplementary information the polarization dependent periodic metasurfaces with the same elements.

Figure 5 shows the cross section of energy at the focal spot at a distance of 10 μm from the metasurfaces for two incident polarizations for 2D random metasurfaces and for the metasurface with a periodic grid. The random 2D metalens is polarization independent as expected while the metasurface with periodic grid and aligned elements is not. However, as previously discussed, the power at the focal spot in Fig. 5(b) is smaller than half the power at the focal spot in Fig. 5(a) and this stems from the differences in near-field interaction configurations.

To further optimize the efficiency of random metasurface, a possible solution would consist in refining the references and use phase-maps representative of the configuration of randomness and accounting for the near-field coupling fluctuation in the metasurface. A local phase method that optimizes the length of elements for quasi periodic metasurfaces has been proven to be effective[53], but it would be very computationally intensive for 2D random metasurfaces. Designing metasurfaces with isotropic elements in the unit cell also leads to polarization
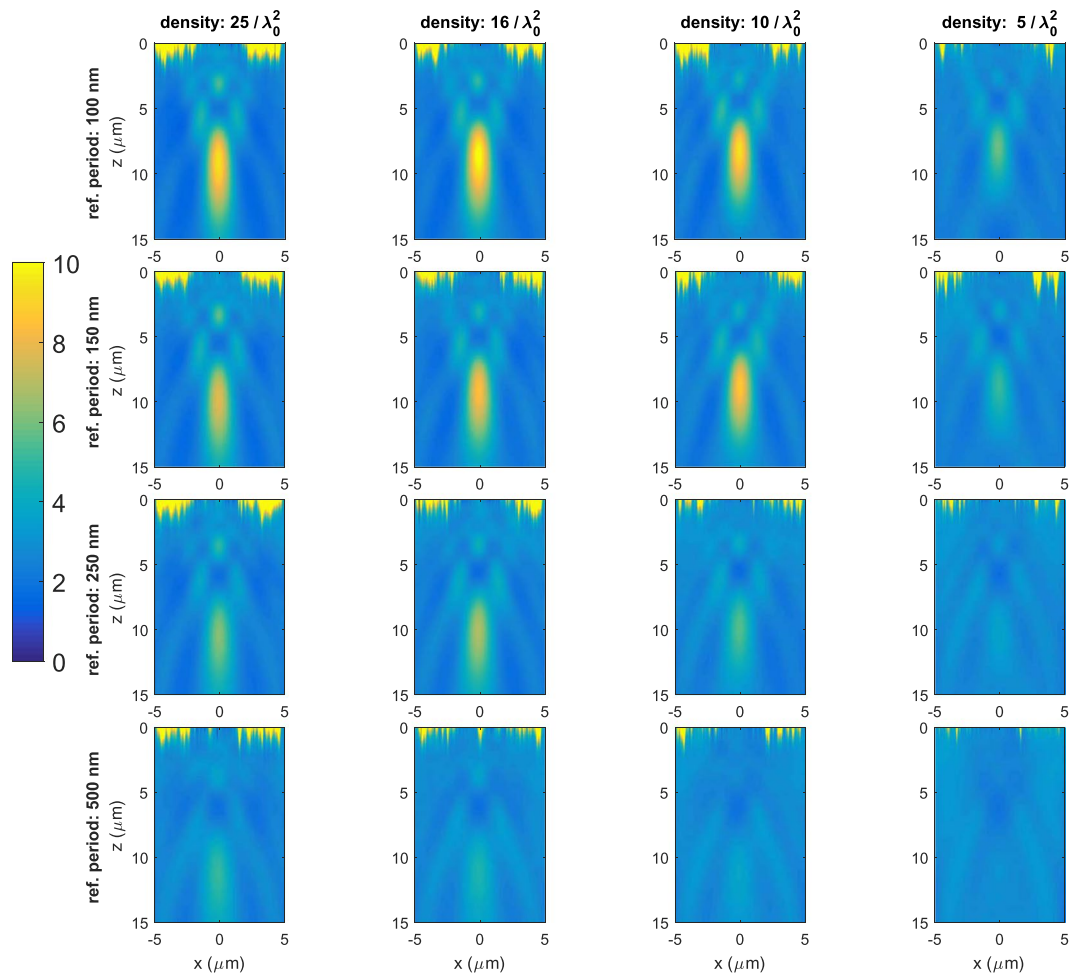
5

Figure 4. Average of the density of energy over 10 samples of 2D random metasurfaces in the xz plane. Influence of the density of elements and reference phase-maps on the focusing of 2D random metalenses for 16 metasurface.

	Metric	Dens. $25/\lambda_0^2$	Dens. $16/\lambda_0^2$	Dens. $10/\lambda_0^2$	Dens. $5/\lambda_0^2$
Ref. period: 100 nm	Max(U)	9.5 ± 1.2	10.3 ± 1.2	9.6 ± 0.8	5.9 ± 0.8
	ΔX (μm)	1.9 ± 0.16	1.9 ± 0.13	1.8 ± 0.17	2.4 ± 0.55
	ΔZ (μm)	8.0 ± 0.25	7.4 ± 0.25	6.8 ± 0.2	6.8 ± 0.5
Ref. period: 150 nm	Max(U)	7.9 ± 0.97	8.5 ± 0.96	9.0 ± 1.2	5.1 ± 0.66
	ΔX (μm)	2.2 ± 0.18	2.1 ± 0.08	2.0 ± 0.19	3.0 ± 0.9
	ΔZ (μm)	8.1 ± 0.25	8.1 ± 0.36	7.4 ± 0.31	8.3 ± 0.63
Ref. period: 250 nm	Max(U)	6.2 ± 0.59	6.9 ± 0.81	5.6 ± 0.51	3.9 ± 0.37
	ΔX (μm)	2.6 ± 0.36	2.5 ± 0.44	2.8 ± 0.38	>5
	ΔZ (μm)	7.8 ± 0.24	8.1 ± 0.20	8.1 ± 0.83	>9.4
Ref. period: 500 nm	Max(U)	5.1 ± 0.64	4.7 ± 0.43	4.0 ± 0.31	3.6 ± 0.24
	ΔX (μm)	>5	>5	>5	>5
	ΔZ (μm)	>9.4	>9.4	>9.4	>9.4

Table 2. Summary of the performances of the 2D random metasurfaces with the mean maximum density of energy, width and length of the focal spots, with their standard deviations.

independence. Whether randomizing such systems can lead to better performance is still an open question. Indeed, the approach presented here could be improved by computing phase-maps of the random structures with randomly placed and oriented identical elements.

Finally, an interesting feature of random metalenses can be seen in Fig. 1(a), the density of elements is not homogeneous. At locations where elements are larger, the density is smaller, while at positions where elements
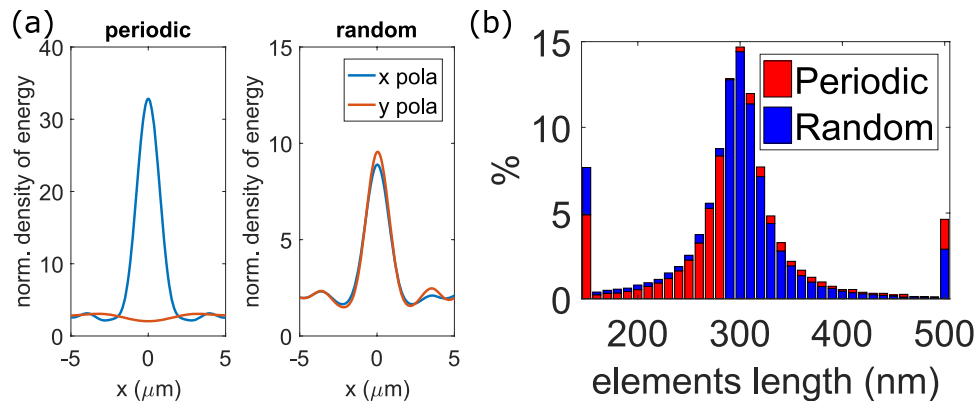
Figure 5. (**a**) Cross sections of the focal spot for a periodic metasurface (left) and the averaged energy of 5 random metasurfaces for the two orthogonal incident polarizations. Metasurfaces correspond to highest density $(25/\lambda_0^2)$ and lowest period for the phase-map (100 nm). (**b**) Distribution of lengths of the 111,000 elements (100 by 100 μm, density of 25 elements/λ_0^2) of a 2D random and the corresponding periodic metasurfaces.

are shorter, the density is higher. Such a distribution can be expected to compensate the fact that smaller elements have a smaller scattering cross-section. Hence, using disordered metalens provides additional degrees of freedom in the design of devices. Figure 5(b) presents the distribution of the length of the elements for a random and a periodic metasurface lens of 100 by 100 μm with a focal length of 250 μm and a density of 25 elements per squared wavelength (111,000 elements on the surface). We can see that a simple random loose packing[60] algorithm favors smaller elements. Such feature may be engineered by tailoring the algorithm used to design the metasurface, for instance using close packing algorithms or hyperuniform media[61–64]. Such algorithms may also be used to explore higher densities.

Conclusion

We proposed a method to design 1D and 2D random metasurface lenses. Using extensive numerical simulations, we demonstrated successful focusing by 1D and 2D random metasurfaces. By implementing random metalenses of various densities using phase-maps of same density (but periodic), we found that the main metric affecting the performance of random 1D metasurfaces is the density of the metasurface, while, in 2D random metasurfaces, the density of the phase-maps or the near-field coupling between elements seems to play a more important role than the density of elements in the metasurface itself. Randomness statistically restores the circular symmetry of the devices and enables polarization independent lenses. We have also demonstrated that random metasurfaces contain a larger number of small scatterers than their periodic counterpart and this may favor higher intensity at the focus if the optimal near-field couplings between random structures is obtained. Further investigations need to be performed to understand the role of the orientation disorder and the strength of the near-field coupling to optimize 2D random metalenses. Our results pave the way to the design of random metasurfaces for devices as diverse as lenses and concentrators. We also believe that random metasurfaces may overcome limitations on the diffraction efficiency of periodic systems, especially for dielectric metasurfaces that are made with larger elements. Random structures are also more amenable to self-assembly fabrication for large scale systems.

Methods

All simulations are performed using the commercially available software CST, version 2017. 1D and 2D metasurface simulations are performed in the time domain for better efficiency. Each layer of materials has an optimized maximum mesh size. It is $\lambda/10$ in air (the domain of the propagation), 15 nm in the gold elements and 30 nm in the SU8 spacer layer. This leads to about 35,000 mesh cells in unit cell simulations, about 16 million for 1D metasurfaces and up to 60 million for 2D metasurfaces. Convergence is ensured by changing the maximum size of the cells to 10 or 20 nm and making sure the results are identical, and, by making sure that energy in the computational volume is monotonously decreasing after the plane wave excitation.

References

1. Huang, J. Reflectarray Antenna. In *Encyclopedia of RF and Microwave Engineering*, https://doi.org/10.1002/0471654507.eme515 (John Wiley & Sons, Inc., 2005).
2. Berry, D., Malech, R. & Kennedy, W. The reflectarray antenna. *IEEE Trans. Antennas Propag.* **11**, 645–651 (1963).
3. Pozar, D. M., Targonski, S. D. & Syrigos, H. D. Design of millimeter wave microstrip reflectarrays. *IEEE Trans. Antennas Propag.* **45**, 287–296 (1997).
4. Encinar, J. A. Design of two-layer printed reflectarrays using patches of variable size. *IEEE Trans. Antennas Propag.* **49**, 1403–1410 (2001).
5. Kaina, N., Dupré, M., Fink, M. & Lerosey, G. Hybridized resonances to design tunable binary phase metasurface unit cells. *Opt. Express* **22**, 18881–18888 (2014).
6. Hsu, L., Lepetit, T. & Kanté, B. Extremely Thin Dielectric Metasurface for Carpet Cloaking. *ArXiv150308486 Phys* (2015).
7. Ni, X., Wong, Z. J., Mrejen, M., Wang, Y. & Zhang, X. An ultrathin invisibility skin cloak for visible light. *Science* **349**, 1310–1314 (2015).
8. Chen, P.-Y. & Alù, A. Mantle cloaking using thin patterned metasurfaces. *Phys. Rev. B* **84**, 205110 (2011).

9. Cheng, J., Jafar-Zanjani, S. & Mosallaei, H. All-dielectric ultrathin conformal metasurfaces: lensing and cloaking applications at 532 nm wavelength. *Sci. Rep.* **6**, 38440 (2016).
10. Ni, X., Kildishev, A. V. & Shalaev, V. M. Metasurface holograms for visible light. *Nat. Commun.* **4**, 3807 (2013).
11. Larouche, S., Tsai, Y.-J., Tyler, T., Jokerst, N. M. & Smith, D. R. Infrared metamaterial phase holograms. *Nat. Mater.* **11**, 3278 (2012).
12. Chen, W. T. *et al*. High-Efficiency Broadband Meta-Hologram with Polarization-Controlled Dual Images. *Nano Lett.* **14**, 225–230 (2014).
13. Yifat, Y. *et al*. Highly Efficient and Broadband Wide-Angle Holography Using Patch-Dipole Nanoantenna Reflectarrays. *Nano Lett.* **14**, 2485–2490 (2014).
14. Huang, L. *et al*. Three-dimensional optical holography using a plasmonic metasurface. *Nat. Commun.* **4**, 3808 (2013).
15. Malek, S. C., Ee, H.-S. & Agarwal, R. Strain Multiplexed Metasurface Holograms on a Stretchable Substrate. *Nano Lett.* **17**, 3641–3645 (2017).
16. Wan, W., Gao, J. & Yang, X. Metasurface Holograms for Holographic Imaging. *Adv. Opt. Mater.* **5**, 1700541 (2017).
17. Zheng, G. *et al*. Metasurface holograms reaching 80% efficiency. *Nat. Nanotechnol.* **10**, 308–312 (2015).
18. Chen, X. *et al*. Dual-polarity plasmonic metalens for visible light. *Nat. Commun.* **3**, 1198 (2012).
19. Khorasaninejad, M. *et al*. Polarization-Insensitive Metalenses at Visible Wavelengths. *Nano Lett.* **16**, 7229–7234 (2016).
20. Lin, D., Fan, P., Hasman, E. & Brongersma, M. L. Dielectric gradient metasurface optical elements. *Science* **345**, 298–302 (2014).
21. Kildishev, A. V., Boltasseva, A. & Shalaev, V. M. Planar Photonics with Metasurfaces. *Science* **339**, 1232009 (2013).
22. Hsu, L., Dupré, M., Ndao, A. & Kanté, B. From parabolic-trough to metasurface-concentrator: assessing focusing in the wave-optics limit. *Opt. Lett.* **42**, 1520–1523 (2017).
23. Wan, C., Chen, L. & Cryan, M. J. Broadband metasurface absorber for solar thermal applications. *J. Opt.* **17**, 125103 (2015).
24. Yu, N. *et al*. Light Propagation with Phase Discontinuities: Generalized Laws of Reflection and Refraction. *Science* **334**, 333–337 (2011).
25. Fu, Y. & Zhou, X. Plasmonic Lenses: A Review. *Plasmonics* **5**, 287–310 (2010).
26. Verslegers, L. *et al*. Planar Lenses Based on Nanoscale Slit Arrays in a Metallic Film. *Nano Lett.* **9**, 235–238 (2009).
27. Aieta, F. *et al*. Aberration-Free Ultrathin Flat Lenses and Axicons at Telecom Wavelengths Based on Plasmonic Metasurfaces. *Nano Lett.* **12**, 4932–4936 (2012).
28. Memarzadeh, B. & Mosallaei, H. Array of planar plasmonic scatterers functioning as light concentrator. *Opt. Lett.* **36**, 2569–2571 (2011).
29. Kanté, B., Lourtioz, J.-M. & de Lustrac, A. Infrared metafilms on a dielectric substrate. *Phys. Rev. B* **80**, 205120 (2009).
30. Genevet, P., Capasso, F., Aieta, F., Khorasaninejad, M. & Devlin, R. Recent advances in planar optics: from plasmonic to dielectric metasurfaces. *Optica* **4**, 139–152 (2017).
31. Arbabi, A., Horie, Y., Bagheri, M. & Faraon, A. Dielectric metasurfaces for complete control of phase and polarization with subwavelength spatial resolution and high transmission. *Nat. Nanotechnol.* **10**, 937–943 (2015).
32. Bomzon, Z., Biener, G., Kleiner, V. & Hasman, E. Space-variant Pancharatnam-Berry phase optical elements with computer-generated subwavelength gratings. *Opt. Lett.* **27**, 1141–1143 (2002).
33. Bomzon, Z., Kleiner, V. & Hasman, E. Computer-generated space-variant polarization elements with subwavelength metal stripes. *Opt. Lett.* **26**, 33–35 (2001).
34. Pancharatnam, S. Generalized theory of interference, and its applications. *Proc. Indian Acad. Sci. - Sect. A* **44**, 247–262 (1956).
35. Berry, M. V. The Adiabatic Phase and Pancharatnam's Phase for Polarized Light. *J. Mod. Opt.* **34**, 1401–1407 (1987).
36. Mosk, A. P., Lagendijk, A., Lerosey, G. & Fink, M. Controlling waves in space and time for imaging and focusing in complex media. *Nat. Photonics* **6**, 283–292 (2012).
37. Pors, A., Ding, F., Chen, Y., Radko, I. P. & Bozhevolnyi, S. I. Random-phase metasurfaces at optical wavelengths. *Sci. Rep.* **6**, 28448 (2016).
38. Shen, Y. *et al*. Phase random metasurfaces for broadband wide-angle radar cross section reduction. *Microw. Opt. Technol. Lett.* **57**, 2813–2819 (2015).
39. Yang, X. M., Jiang, G. L., Liu, X. G. & Yang, J. F. RCS reduction by metasurface with random distribution of reflection phases. In *2015 IEEE MTT-S International Microwave Workshop Series on Advanced Materials and Processes for RF and THz Applications* (*IMWS-AMP*) 1–3, https://doi.org/10.1109/IMWS-AMP.2015.7324988 (2015).
40. Su, P., Zhao, Y., Jia, S., Shi, W. & Wang, H. A broadband random metasurface for Radar Cross Section reduction. In *2015 Asia-Pacific Microwave Conference* (*APMC*) **2**, 1–3 (2015).
41. Nishijima, Y., Khurgin, J. B., Rosa, L., Fujiwara, H. & Juodkazis, S. Randomization of gold nano-brick arrays: a tool for SERS enhancement. *Opt. Express* **21**, 13502–13514 (2013).
42. Ling, X., Luo, H., Zhao, C., Wen, S. & Fan, D. Metamaterial-based polarization control plate for producing incoherent laser irradiation. *Appl. Opt.* **51**, 4749–4753 (2012).
43. Florescu, M., Torquato, S. & Steinhardt, P. J. Designer disordered materials with large, complete photonic band gaps. *Proc. Natl. Acad. Sci.* **106**, 20658–20663 (2009).
44. Vynck, K., Burresi, M., Riboli, F. & Wiersma, D. S. Photon management in two-dimensional disordered media. *Nat. Mater.* **11**, nmat3442 (2012).
45. Lee, W.-K. *et al*. Concurrent design of quasi-random photonic nanostructures. *Proc. Natl. Acad. Sci.* **114**, 8734–8739 (2017).
46. Lemoult, F., Lerosey, G., de Rosny, J. & Fink, M. Manipulating Spatiotemporal Degrees of Freedom of Waves in Random Media. *Phys. Rev. Lett.* **103**, 173902 (2009).
47. Jang, M. *et al*. Complex wavefront engineering with disorder-engineered metasurfaces. *ArXiv170608640 Phys* (2017).
48. Veksler, D. *et al*. Multiple Wavefront Shaping by Metasurface Based on Mixed Random Antenna Groups. *ACS Photonics* **2**, 661–667 (2015).
49. Qiao, P., Zhu, L. & Chang-Hasnain, C. High-efficiency aperiodic two-dimensional high-contrast-grating hologram. *Proc. SPIE High Contrast Metastructures* V 9757, (2016).
50. Andryieuski, A., Lavrinenko, A. V., Petrov, M. & Tretyakov, S. A. Homogenization of metasurfaces formed by random resonant particles in periodical lattices. *Phys. Rev. B* **93**, 205127 (2016).
51. Albooyeh, M., Morits, D. & Tretyakov, S. A. Effective electric and magnetic properties of metasurfaces in transition from crystalline to amorphous state. *Phys. Rev. B* **85**, 205110 (2012).
52. Helgert, C. *et al*. Effective properties of amorphous metamaterials. *Phys. Rev. B* **79**, 233107 (2009).
53. Hsu, L., Dupré, M., Ndao, A., Yellowhair, J. & Kanté, B. Local phase method for designing and optimizing metasurface devices. *Opt. Express* **25**, 24974–24982 (2017).
54. Lalanne Philippe & Chavel Pierre. Metalenses at visible wavelengths: past, present, perspectives. *Laser Photonics Rev.* **11**, 1600295 (2017).
55. Kante, B., O'Brien, K., Niv, A., Yin, X. & Zhang, X. Proposed isotropic negative index in three-dimensional optical metamaterials. *Phys. Rev. B* **85**, 041103 (2012).
56. Chong, K. E. *et al*. Efficient Polarization-Insensitive Complex Wavefront Control Using Huygens' Metasurfaces Based on Dielectric Resonant Meta-atoms. *ACS Photonics* **3**, 514–519 (2016).
57. Arbabi, E., Arbabi, A., Kamali, S. M., Horie, Y. & Faraon, A. Multiwavelength polarization-insensitive lenses based on dielectric metasurfaces with meta-molecules. *Optica* **3**, 628–633 (2016).

58. Arbabi, A., Horie, Y., Ball, A. J., Bagheri, M. & Faraon, A. Subwavelength-thick lenses with high numerical apertures and large efficiency based on high-contrast transmitarrays. *Nat. Commun.* **6**, 7069 (2015).
59. Johnson, P. B. & Christy, R. W. Optical Constants of the Noble Metals. *Phys. Rev. B* **6**, 4370–4379 (1972).
60. Delaney, G. W., Hilton, J. E. & Cleary, P. W. Defining random loose packing for nonspherical grains. *Phys. Rev. E* **83**, 051305 (2011).
61. Kurita, R. Experimental study of random-close-packed colloidal particles. *Phys. Rev. E* **82** (2010).
62. Katzav, E., Adda-Bedia, M. & Boudaoud, A. A statistical approach to close packing of elastic rods and to DNA packaging in viral capsids. *Proc. Natl. Acad. Sci.* **103**, 18900–18904 (2006).
63. Degl'Innocenti, R. *et al.* Hyperuniform disordered terahertz quantum cascade laser. *Sci. Rep.* **6**, srep19325 (2016).
64. Torquato, S. Hyperuniformity and its generalizations. *Phys. Rev. E* **94**, 022122 (2016).

Acknowledgements

Author Contributions

B. Kanté conceived the project. M. Dupré designed the structures and performed the simulations. All authors discussed the results, analyzed the data, and wrote the manuscript.

Additional Information

Supplementary information accompanies this paper at https://doi.org/10.1038/s41598-018-25488-4.

Competing Interests: The authors declare no competing interests.

Publisher's note: Springer Nature remains neutral with regard to jurisdictional claims in published maps and institutional affiliations.